J Nanopart Res (2014) 16:2392
DOI 10.1007/s11051-014-2392-4

RESEARCH PAPER

Thermochemical behavior of nano-sized aluminum-coated nickel particles

Dilip Srinivas Sundaram · Puneesh Puri ·
Vigor Yang

Received: 17 September 2013 / Accepted: 28 March 2014

Abstract Molecular dynamics simulations are performed to investigate the thermochemical behavior of aluminum-coated nickel particles in the size range of 4–13 nm, beyond which asymptotic behavior is observed. The atomic interactions are captured using an embedded atom model. Emphasis is placed on the particle melting behavior, diffusion characteristics, and inter-metallic reactions. Results are compared with the corresponding properties of nickel-coated nano-aluminum particles. Melting of the shell, which is a heterogeneous process beginning at the outer surface of the particle, is followed by diffusion of aluminum and nickel atoms and inter-metallic reactions. The ensuing chemical energy heats up the particle under adiabatic conditions. The alloying reactions progressively transform the core–shell structured particle into a homogeneous alloy. The melting temperature of the shell is weakly dependent on the core size, but increases significantly with increasing shell thickness, from 750 K at 1 nm to 1,000 K at 3 nm. The core melts at a temperature comparable to the melting point of a nascent particle, contrary to the phenomenon of superheating observed for nickel-coated aluminum particles. The melting temperature of the core decreases from 1,730 to 1,500 K, when its diameter decreases from 10 to 7 nm. For smaller cores, the majority of nickel atoms participate in reactions before melting. The diffusion coefficient of nickel atoms in aluminum shell exhibits a temperature dependence of the form $D = D_0 \exp(-E_A/RT)$, with an activation energy of 43.65 kJ/mol and a pre-exponential factor of 1.77×10^{-7} m^2/s. The adiabatic reaction temperature, also a size-dependent quantity, increases with increasing core diameter, attains a maximum value of 2,050 K at 5 nm, and decreases with further increase in the core diameter. The calculated values agree reasonably with those obtained via chemical equilibrium analysis. The burning time exhibits strong dependence of particle core size and shell thickness of the form $\tau_b = a\, d_c^n\, \delta_s^m$, where the exponents n and m are 1.70 and 1.38, respectively. The finding further corroborates the fact that the reaction rate is controlled by diffusion process.

Keywords Nano-nickel particle · Nano-aluminum particle · Inter-metallic diffusion and reaction · Metal particle thermodynamics

List of symbols

A	Area
Al	Aluminum
C_p	Specific heat
D	Diffusion coefficient
d	Diameter

D. S. Sundaram · V. Yang (✉)
School of Aerospace Engineering, Georgia Institute of Technology, Atlanta, GA 30332, USA
e-mail: vigor.yang@aerospace.gatech.edu

P. Puri
Department of Mechanical and Nuclear Engineering,
The Pennsylvania State University, University Park,
State College, PA, USA

E_A	Activation energy
F	Force
H	Enthalpy
k_B	Boltzmann constant
M	Mass
m	Thickness exponent, mass
N	Number of atoms
n	Diameter exponent
Ni	Nickel
P	Pressure
q	Generalized coordinate
Q	Inertia factor
R	Gas constant
r	Position vector, radius
s	Thermostat degree of freedom
T	Temperature
t	Thickness
U	Potential energy
V	Volume, pair potential function

Greek

ρ	Electron density function
δ_s	Shell thickness
δ_t	Thermal displacement
τ_b	Burning time

Subscripts

ad	Adiabatic
c	Core
cm	Center of mass
f	Formation
i	Initial, interface, atom index variable
j	Atom index variable
m	Melting
p	Particle
prod	Products
reac	Reactants

Introduction

Energetic materials composed of nickel and aluminum have been employed in various propulsion and pyrotechnic applications (Andrzejak et al. 2007; Reeves et al. 2010; Fischer and Grubelich 1996). They are employed as localized heat sources for chemical and bio neutralization, ultrafast fuses, and smart thermal barriers (Zhao et al. 2006). Nickel–aluminum (Ni–Al) system is ideal for situations in which liberation of gas-phase products is not desired, since the reaction yields only condensed-phase products. Table 1 shows the heat of reaction and adiabatic reaction temperature for some of the most energetic aluminum-based intermetallic reactions (Morsi 2001; Meschel and Kleppa 2001; Fischer and Grubelich 1998). The adiabatic reaction temperature of Ni–Al reaction is as high as 1,911 K, greater than those of other reactions, with the exception of Pd–Al and Pt–Al counterparts. These demonstrate the high energy content of the Ni–Al system.

Table 1 Heat of reaction and adiabatic reaction temperature of aluminum-based inter-metallic reactions (Morsi 2001; Meschel and Kleppa 2001; Fischer and Grubelich 1998)

Reaction	Heat of reaction (kJ/mol)	Reaction temperature, K ($T_{\text{initial}} = 298$ K)
$3Ni + Al \rightarrow Ni_3Al$	−153.1	1,586
$Ni + Al \rightarrow NiAl$	−118.4	1,911
$2Ni + 3Al \rightarrow Ni_2Al_3$	−282.4	1,406
$Ni + 3Al \rightarrow NiAl_3$	−150.7	1,127
$Pt + Al \rightarrow PtAl$	−200.4	3,073
$Pd + Al \rightarrow PdAl$	−183.8	2,653
$Ti + 3Al \rightarrow TiAl_3$	−146.4	1,591
$Fe + Al \rightarrow FeAl$	−47.0	1,423

Consolidated blends of aluminum and nickel powders are widely used in the combustion synthesis of nickel aluminides (Ni_xAl_{1-x}), which are attractive structural materials for a variety of engineering systems (Morsi 2001). The reactant powders are ignited at one end and a self-sustaining combustion wave propagates through the packed mixture. The profound interest in the combustion synthesis lies in the simplicity and cost effectiveness of the process (Aruna and Mukasyan 2008). The combustion products have relatively low impurity content, since the flame vaporizes volatile contaminants (Li 2003). The efficiency of the process can be further enhanced by employing nano-sized particles (Hunt et al. 2004), which have unusually favorable physicochemical properties due to the presence of a large number of atoms on the particle surface. The melting temperature of a 2-nm aluminum particle is 473 K, which is lower than the bulk value of 933 K by 460 K (Puri and Yang

2007). The ignition temperatures and burning times of nano-aluminum particles are also lower than those of their micron-sized counterparts (Huang et al. 2009). Micro-structural images of the powder blend indicate that the nickel particles are embedded in a continuous aluminum matrix or vice versa (Farber et al. 1998). The geometry of such a system can, thus, be simplified as a core–shell particle structure, where the shell represents the surrounding matrix (Farber et al. 1998). Furthermore, Ni/Al clad particles can be directly employed to synthesis nickel aluminides (Thiers et al. 2002). Understanding their physicochemical characteristics is, thus, of paramount importance to material synthesis applications.

A common approach to synthesize Ni/Al core–shell structured particles is the solution process (Foley et al. 2005). Nascent metal particles are slurried with dimethyl ether (DME) solvent. In a separate flask, a chemical complex of the coating metal is dissolved in DME. The resulting solution is added to the stirred metal slurry and allowed to react at room temperature for 12 h. This process results in the formation of uniform coating on the parent metal particle. Another synthesis technique is the cyclic electroplating process (Yih 2000). The particles are immersed in a metal ion containing electrolyte, stirred, and allowed to sediment loosely on the cathode plate. An electric potential is applied across the anode and cathode plates to deposit metallic ions in the electrolyte on the particle surface.

Molecular dynamics (MD) simulations of planar Ni–Al systems have been recently performed (Baras and Politano 2011; Politano et al. 2013). In our previous work (Sundaram et al. 2013), the effects of core size and shell thickness on the thermochemical behavior of spherical nickel-coated nano-aluminum particles were investigated. For aluminum-coated nickel particles, such studies are yet to be performed. Previous works (Henz et al. 2009; Levchenko et al. 2010) considered particles with equal numbers of aluminum and nickel atoms. From a purely scientific perspective, a comparative analysis of the physicochemical properties of these two different systems is interesting and useful. The present investigation will address these issues by means of MD simulations. Emphasis is placed on the particle melting behavior, diffusion processes, and inter-metallic reactions. The core diameter covers a range of 2–10 nm, and four different shell thicknesses of 0.5, 1.0, 2.0, and 3.0 nm are chosen.

Theoretical framework

The basis of the present work is the general analysis outlined in our previous work (Sundaram et al. 2013). The atomic interactions are reproduced using an embedded atom potential function with the parameters developed by Papanicolaou et al. (2003). The potential energy (U) can be expressed as

$$U=\sum_{i=1}^{N}\left\{\sum_{j}A_{\alpha\beta}e^{-p_{\alpha\beta}\left(\frac{r_{ij}}{r^{0}_{\alpha\beta}}-1\right)}-\left[\sum_{j}\xi^{2}_{\alpha\beta}e^{-2q_{\alpha\beta}\left(\frac{r_{ij}}{r^{0}_{\alpha\beta}}-1\right)}\right]^{1/2}\right\}, \tag{1}$$

where r_{ij} represents the distance between atoms i and j and N is the number of atoms. Table 2 lists the parameters of the model. They were obtained by fitting the potential function to the properties of aluminum, nickel, and nickel-aluminum ordered alloys. For particles considered in the present work, phase-equilibrium analysis suggests that the reaction products are B2-NiAl and Al-rich species (e.g., $NiAl_3$). It is reassuring to note that the potential function reproduces the properties of these materials with reasonable accuracy.

Isobaric–isothermal (NPT) ensemble is used to study melting and diffusion processes in the presence of external heating at constant pressure conditions. The equations of motion are given by (Andersen 1980; Nose 1984)

$$\begin{aligned}
M\ddot{V}&=-P+\frac{s^{2}}{3V}\left[V^{2/3}\sum_{i}m_{i}\dot{q}_{i}^{2}-V^{1/3}\sum_{i}F_{i}q_{i}\right]\\
m_{i}\ddot{q}_{i}&=\frac{V^{-1/3}F_{i}}{s^{2}}-\frac{2m_{i}\dot{V}\dot{q}_{i}}{3V}-\frac{2m_{i}\dot{s}\dot{q}_{i}}{s}\\
Q\ddot{s}&=sV^{2/3}\sum_{i}m_{i}\dot{q}_{i}^{2}-\frac{gk_{B}T}{s}
\end{aligned} \tag{2}$$

where q_i is the generalized coordinate, $\dot{q}_i$ and $\ddot{q}_i$ denote the first-order and second-order derivatives of q_i with

Table 2 Parameters of the embedded atom potential function (Papanicolaou et al. 2003)

	Ni–Ni	Al–Al	Ni–Al
A (eV)	0.0741	0.0550	0.0949
ξ (eV)	1.4175	0.9564	1.4677
p	13.8297	10.9011	10.9486
q	2.2448	1.5126	3.8507
r_0 (Å)	2.4307	2.8310	2.7424

respect to time, F_i is the net force on atom i, M is the fictitious mass for volume motion, m is the mass of the atom, V is the volume, P is the pressure, T is the temperature, Q is the thermal inertia factor, g is a parameter, k_B is the Boltzmann constant, and s is the additional degree of freedom. Isochoric–isoenergetic (NVE) ensemble is employed to investigate self-heating of the particle due to inter-metallic reactions under adiabatic conditions. For the NVE ensemble, the equations of motion can be written as

$$m_i \ddot{q}_i = -\frac{\partial U}{\partial q_i} \tag{3}$$

The equations of motion are numerically integrated using a fifth-order predictor–corrector algorithm. The time step is chosen as 1 fs in order to capture the vibrational motion of the atoms accurately. Negligible improvement in the model results is obtained when the time step is reduced from 1 to 0.1 fs. The heating rate is chosen as 10^{-2} K/fs based on the results of a parametric study conducted in our previous work (Sundaram et al. 2013). Heating rates lower than 10^{-2} K/fs increases the total computational time dramatically with only little change in the model results.

Results and discussion

Melting of nascent aluminum and nickel particles

The theoretical framework is first employed to analyze melting of nascent aluminum and nickel particles. Figure 1a shows the variation of potential energy with temperature for a 9-nm aluminum particle consisting of 23,328 atoms. A gradual deviation from the initial linear trend at about 900 K marks the onset of surface melting of the particle. The potential energy difference can be calculated as follows:

$$\Delta E(n) = E(n+m) - E(n), \tag{4}$$

where E is the potential energy and n is the integration step number. The constant, m, is chosen so as to determine the melting point within an accuracy of ±25 K. The result is shown in Fig. 1b. The surface melting begins at 900 K, as evidenced by an abrupt increase in the potential energy difference. The peak melting rate occurs at 1,075 K and phase transition is complete at 1,200 K. It is important to recognize that nano-particle melts over a range of temperatures, as opposed to isothermal structural melting of surface-free bulk materials. Note that the melting temperature range increases with increasing heating rate (Sundaram et al. 2013). Figure 2 shows the effect of particle size on the melting temperature of aluminum and nickel particles. The model predictions are compared with the results of previous MD simulations (Puri and Yang 2007; Sundaram et al. 2013; Qi et al. 2001) and experiments (Eckert et al. 1993; Lai et al. 1998). The size dependence of melting temperature of nano-particles is well described by the Gibbs-Thompson theory

$$T_m(r) = T_m^b - \left(\frac{2T_m^b \sigma_{sl}}{H_f^b \rho_s r}\right), \tag{5}$$

where T_m is the melting temperature, H_f is the latent heat of fusion, ρ_s is the solid phase density, and r is the particle radius. The subscript b refers to the bulk material. The resulting values are also shown in the figure. Note that more sophisticated models that couple phase-field theory to material mechanics have been developed recently (Levitas and Samani 2011). The predicted melting temperatures are greater than those obtained using the Cleri–Rosato potential function (Sundaram et al. 2013), but agree reasonably well with the counterparts of the glue potential (Puri and Yang 2007). In the experiments, particle melting was studied using differential scanning calorimetry (DSC) (Eckert et al. 1993) and thin-film DSC (Lai et al. 1998) setups, with heating rates on the order of 1 and 10^5 K/s, respectively. These are orders of magnitude lower than the heating rate employed in the present MD simulations. The melting point increases with increasing heating rate (Lu and Ahrens 2003). Furthermore, the experiments considered passivated particles, while the present study deals with nascent particles. It is well known that that passivated particles exhibit the phenomenon of superheating (Mei and Lu 2007). For homogeneous melting, the degree of superheating increases with decreasing particle size (Mei and Lu 2007). It is, thus, not surprising that the predicted melting points are greater than the experimental data, especially for large particle sizes. Note that the measured values of Eckert et al. (1993) and Lai et al. (1998) are different. This may be attributed to the differences in the heating rate and fabrication methods. Lai et al.'s particles were prepared using vapor-phase condensation method, whereas Eckert et al.

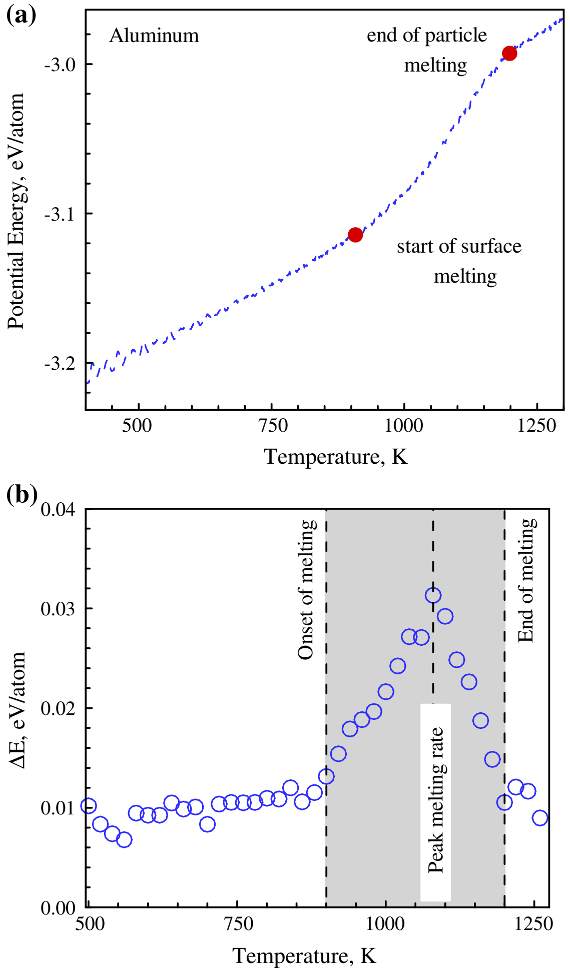

Fig. 1 **a** Variation of potential energy with temperature for a 9-nm aluminum particle consisting of 23,328 atoms, **b** potential energy difference as a function of temperature showing the onset and completion of particle melting

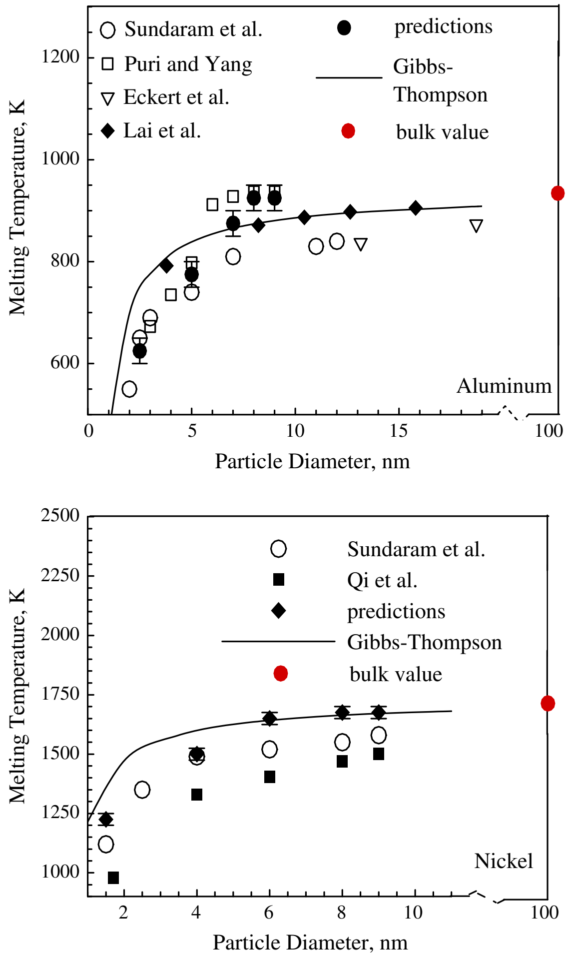

Fig. 2 Effect of particle size on the melting temperature of aluminum and nickel particles

employed mechanical attrition technique. Figure 2b shows the melting temperature of nickel particles calculated by Qi et al. (2001) using the quantum Sutton–Chen force field. They are significantly lower than the values obtained in the present work. As can be seen, the embedded atom model with the parameters developed by Papanicolaou et al. (2003) offers accurate predictions of the melting temperature of aluminum and nickel particles.

Thermochemical behavior of aluminum-coated nickel particles

The thermochemical behavior of aluminum-coated nickel particles is investigated for different core diameters and shell thicknesses. Emphasis is placed on the particle melting behavior, diffusion characteristics, and inter-metallic reactions. The particle is generated by inserting the nickel core into a spherical cavity created in the aluminum particle. Figure 3 shows a snapshot of the particle cross-section. The particle is equilibrated at a temperature of 300 K. It is then heated at a constant rate of 0.01 K/fs. Figure 4 shows the temporal variation of the core radius and potential energies of the core and shell during equilibration simulation. After an initial transient phase, the parameters attain their respective equilibrium value. Table 3 shows the core diameter (d_c), shell thickness (δ_s), total number of atoms (N), and number of nickel atoms (N_{Ni}) of the particles chosen in the present study. The core diameter covers the range of

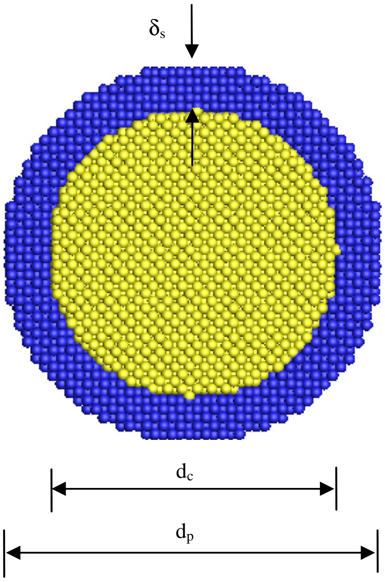

Fig. 3 Snapshot of a dissected aluminum-coated nickel particle ($d_p = d_c + 2\delta_s$)

2–10 nm and four different shell thicknesses of 0.5, 1.0, 2.0, and 3.0 nm are considered. Figure 5 shows the key physicochemical processes during heating of aluminum-coated nickel particles. The time period of concern can be divided into four stages based on phase transitions and inter-metallic reactions. In the first stage, the particle is heated to the melting point of the aluminum shell. Solid-state diffusion is predominant in this stage. Melting of the aluminum shell, which marks the onset of the second stage, facilitates the dissolution of nickel atoms. In the third stage, diffusion of aluminum and nickel atoms becomes more prominent. It transforms the core–shell particle into a homogeneous alloy. The ensuing exothermic inter-metallic reactions significantly heats up the particle. In the following sections, the aforementioned physicochemical processes are discussed in detail.

Melting of shell

The bulk melting temperature of aluminum shell is 933 K, which is significantly lower than that of nickel core (1,728 K). For aluminum-coated nickel particles, the shell thus melts before the core. In the present study, the melting point is determined based on the variation of the potential energy with temperature. This is shown in Fig. 6. The onset of melting is characterized by a gradual deviation of the potential energy from the linear trend. For a particle with a core diameter of 3 nm and shell thickness of 2 nm, the melting temperature is predicted to be 930 K. Note that the ensuing decrease in the potential energy can be attributed to nickel–aluminum reactions.

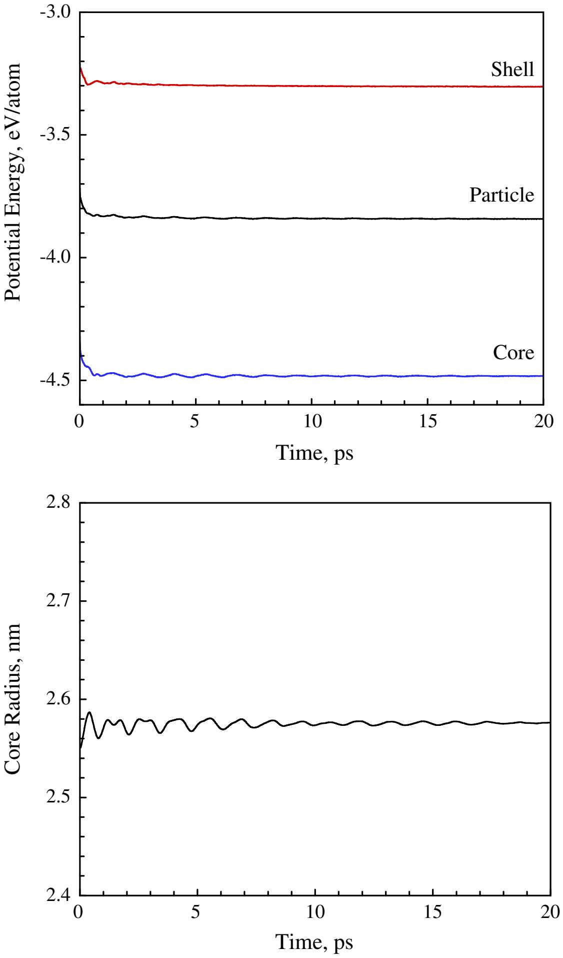

Fig. 4 Variation of potential energy and core radius with time during particle equilibration at a temperature of 300 K

It is important to understand the mechanism of melting of the shell. This can be accomplished by monitoring the radial variation of a suitable structural or thermodynamic parameter. Figure 7 shows the snapshots of the dissected particle colored by thermal displacement of the shell atoms. The atomic thermal displacement is given by

$$\delta_{t,i} = \sqrt{\left(r_i - r_{0,i}\right)^2}, \tag{6}$$

where r denotes the position vector. The subscripts i and 0 refer to atom i and the initial state, respectively.

Table 3 Configuration of aluminum-coated nickel particles

Core diameter (d_c), nm	Shell thickness (δ_s), nm	Total number of atoms (N)	Number of nickel atoms (N_{Ni})
2	1.0	2,321	342
2	2.0	7,430	342
3	0.5	1,919	874
3	1.0	3,715	874
3	2.0	10,252	874
3	3.0	21,954	874
5	0.5	9,642	6,379
5	1.0	13,973	6,379
5	2.0	27,099	6,379
7	1.0	27,832	15,499
7	2.0	47,082	15,499
7	3.0	74,675	15,499
10	1.0	79,233	53,754

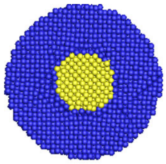

Stage – I (solid-state diffusion)

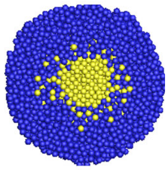

Stage – II (shell melting and dissolution of core atoms)

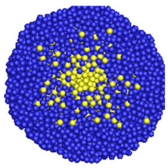

Stage – III (diffusion and inter-metallic reactions)

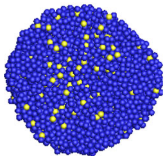

Stage – IV (heating of alloyed particle)

Fig. 5 Key physicochemical processes during heating of nano-sized aluminum-coated nickel particles

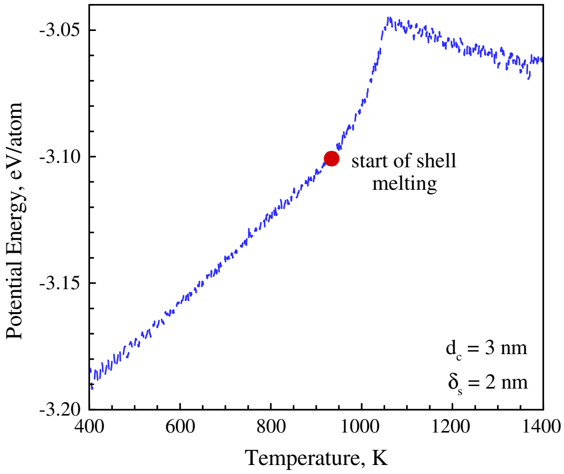

Fig. 6 Potential energy of the shell as a function of temperature for a particle with core diameter of 3 nm and shell thickness of 2 nm

The thermal displacement is a measure of lattice disorder induced by thermal motion. It is expected to increase abruptly during melting. The snapshots indicate that the shell melting is a heterogeneous process in which the nucleation of the liquid phase begins at the outer surface of the particle. The melting front propagates toward the core–shell interface with increasing temperature.

Particle core diameter and shell thickness are the two important parameters that affect the melting point of the shell. Figure 8 shows the variation of the melting temperature of the shell with the core diameter for a shell thickness of 2 nm. The core size exerts a weak effect on the melting temperature of the shell in the size range of 2–7 nm. Figure 9 shows the effect of shell thickness on the melting temperature of the shell for a core diameter of 7 nm. It increases with increasing shell thickness, from 750 K at 1 nm to 1,000 K at 3 nm. A qualitatively similar trend was observed for other values of core diameters considered in the present study. A thicker shell typically melts at a higher temperature, since the percentage of surface atoms in the shell decreases with increasing shell thickness. Note that the melting point is weakly dependent on the shell thickness, when the latter exceeds 2 nm. In order to understand the observed trends, it is imperative to explore the dependencies of the surface-area-to-volume ratio (SVR) of the shell on core diameter and shell thickness.

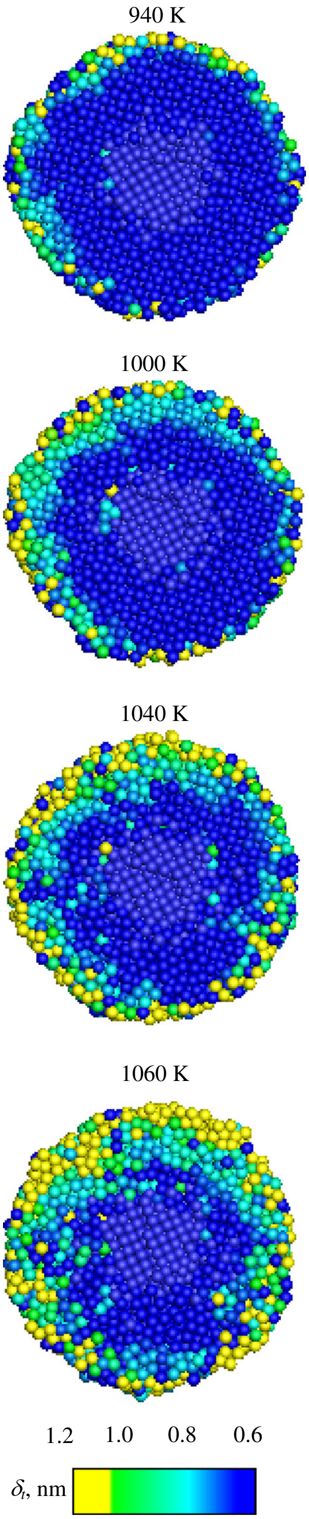

Fig. 7 Snapshots of the particle colored by thermal displacement of aluminum atoms

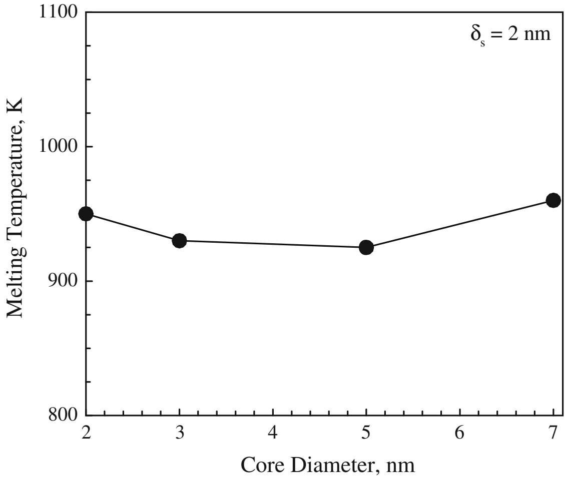

Fig. 8 Effect of core diameter on the melting temperature of the shell for particles with a shell thickness of 2 nm

$$\mathrm{SVR}_{\mathrm{core}} = \frac{3}{r}, \tag{7}$$

$$\mathrm{SVR}_{\mathrm{shell}} = \frac{3R^2}{R^3 - r^3}, \tag{8}$$

where r is the core radius and R is the particle radius. The results are shown in Fig. 10. An asymptotic behavior is observed when the characteristic dimension attains a critical value. The critical values of core radius and shell thickness are 4 and 2 nm, respectively. Furthermore, the surface-area-to-volume ratio of the core increases by an order of magnitude, when the core diameter decreases from 10 to 1 nm. For a spherical shell, it increases only by a factor of two. These clearly explain the weak dependence of the shell melting point on core size and asymptotic melting behavior for shell thickness exceeding 2 nm. Deviation of the melting temperature of the shell from its bulk value is negligible for shell thickness greater than 3 nm.

Diffusion process

Melting of the shell is followed by outward diffusion of nickel atoms. In order to study the diffusion of nickel atoms, the core radius is calculated as follows:

$$r_{\mathrm{c}} = \sqrt{\frac{5}{3N_{\mathrm{Ni}}}\sum_{i=1}^{N_{\mathrm{Ni}}}\left(r_i - r_{\mathrm{cm}}\right)^2}, \tag{9}$$

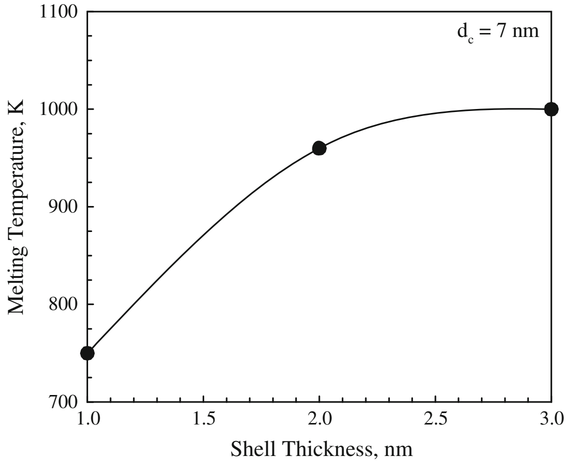

Fig. 9 Effect of shell thickness on the melting temperature of shell for particles with a core diameter of 7 nm

where r_{cm} is the position vector of the center of mass. Figure 11a shows the variation of the core radius with temperature for particles with a core diameter of 3 nm and two different shell thicknesses of 1 and 2 nm. The core radius increases sharply upon melting of the shell, which implies that the diffusion of nickel atoms is a consequence of shell melting phenomenon. Diffusion and ensuing inter-metallic reactions are naturally promoted for thinner shells, since the melting temperature of the shell decreases with decreasing shell thickness. Figure 11b shows the trends for particles with core diameters in the range of 3–7 nm and shell thickness of 2 nm. The core size exerts only a weak effect on the diffusion process, since the melting temperature of the shell is not a strong function of the core diameter.

The inward diffusion of aluminum atoms is another phenomenon of interest. To facilitate analysis of this phenomenon, the particle is divided into eight spherical layers of thickness 0.5 nm, as shown in Fig. 12. Figure 13 shows the numbers of nickel and aluminum atoms in each layer as a function of temperature for a particle with a core diameter of 5 nm and shell thickness of 1 nm. Layers 1–5 refer to the nickel core and 6–8 the aluminum shell, respectively. The atom distributions change negligibly over the temperature range of 300–800 K. At 1,200 K, nickel atoms beneath the interface diffuse into the shell, and vice versa for aluminum atoms. The diffusion process is thus bidirectional in aluminum-coated nickel particles. Note that the nickel and aluminum atoms are distributed almost uniformly in the particle, and a homogeneous Ni–Al alloy is formed at 2,000 K.

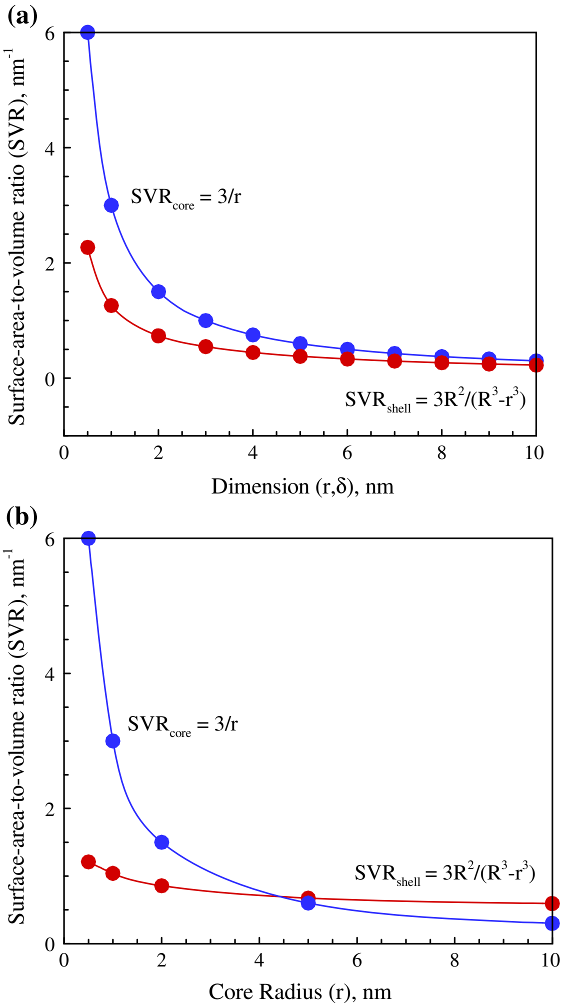

Fig. 10 Variations of surface-area-to-volume ratio (SVR) of the core and shell with **a** core radius and shell thickness for a core diameter of 7 nm; **b** core radius for a shell thickness of 2 nm

The diffusion coefficient of nickel atoms in the aluminum shell is an important property, especially from the standpoint of development of macro-scale models for ignition and combustion. Figure 14 shows the effect of temperature on the diffusion coefficient of nickel atoms for core diameters in the range of 2–7 nm and three different shell thicknesses of 0.5, 1.0, and 2.0 nm. The diffusion coefficient decreases with increasing core diameter, from 1.0 Å^2/ps at 2 nm to 0.33 Å^2/ps at 7 nm for a temperature of 1,600 K. The predictions are comparable to the estimates of Du et al.

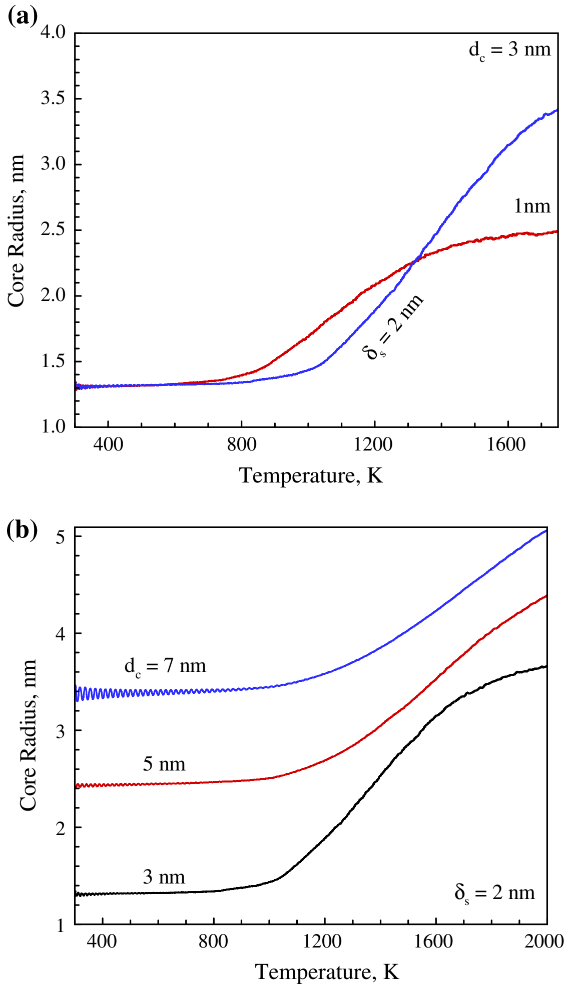

Fig. 11 Core radius as a function of temperature for particles with **a** core diameter of 3 nm and shell thicknesses of 1 and 2 nm; **b** shell thickness of 2 nm and core diameters of 3, 5, and 7 nm

(2003), which in turn is benchmarked against experimental data at macro scales (Ejima et al. 1980; Praizey et al. 2000). The diffusion coefficient exhibits a temperature dependence of the form

$$D = D_0 \exp\left(-\frac{E_A}{RT}\right), \tag{10}$$

where E_A is the activation energy and D_0 is the pre-exponential factor. The curve-fit indicates a value of 43.65 kJ/mol for the activation energy and 1.77×10^{-7} m^2/s for the pre-exponential factor in the temperature range of 1,000–2,000 K. It is important to note that the diffusion coefficients of aluminum atoms are nearly equal to those of nickel atoms. For example, at a particle size of 7 nm, the diffusion coefficient of aluminum atoms increases from 0.5 to 1.67 Å^2/ps, when the temperature increases from 1,000 to 2,000 K. For temperatures lower than 700 K, the diffusion coefficients are in the range of 10^{-3} to 10^{-2} Å^2/ps, significantly lower than the liquid-phase counterparts.

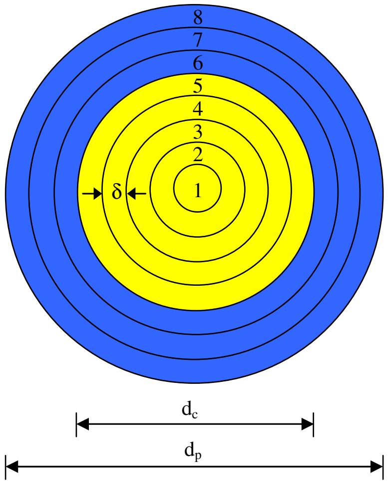

Fig. 12 Schematic of a dissected aluminum-coated nickel particle divided into eight spherical layers of thickness $\delta = 0.5$ nm

Melting of core

It was difficult to clearly ascertain the melting temperature of the core, especially for smaller core sizes. The alloying reactions, which transform the nickel core into an alloyed particle, compete with the core melting process. Figure 15 shows the potential energy of the nickel core as a function of temperature for a particle with core diameter of 10 nm and shell thickness of 1 nm. The core begins to melt at a temperature of 1,730 K, which is nearly the bulk melting point of nickel. The melting temperature of the core decreases with decreasing core diameter, from 1,730 K at 10 nm to 1,500 K at 7 nm. For smaller cores, majority of the nickel atoms participate in alloying reactions before melting. Note that the predicted core melting behavior differs from that observed for nickel-coated aluminum particles. The solid nickel shell exerted a cage-like effect on the aluminum core. As a result, the melting temperature of the core was greater than that of a nascent aluminum

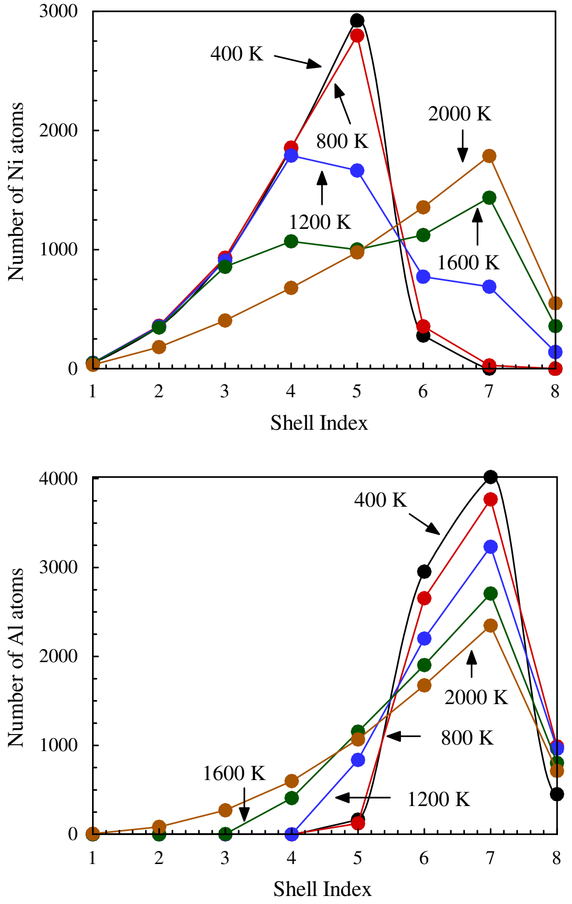

Fig. 13 Number of nickel and aluminum atoms in different spherical shells as a function of temperature for a core diameter of 5 nm and shell thickness of 1 nm

particle (Sundaram et al. 2013). For aluminum-coated nickel particles, no such phenomenon is observed, since the shell melts before the core. The core melts at a temperature comparable to its counterpart of a nascent nickel particle.

Inter-metallic reactions

The diffusion of nickel and aluminum atoms results in exothermic nickel-aluminum reactions, which significantly heats up the particle under adiabatic conditions. Figure 16 shows the variation of the potential energy as a function of temperature for a particle with a core diameter of 3 nm and shell thickness of 2 nm. The potential energy increases, attains a plateau and then again increases. The trend is characteristic of the core–shell particle structure, and is not observed for nascent metal particles. The initial rise in the potential energy is caused by the transfer of energy from the heat reservoir to the particle. The plateau represents the stage at which the energy supply is counterbalanced by the chemical energy release due to intermetallic reactions. The ensuing increase in the potential energy suggests the formation of a homogeneous nickel–aluminum alloy.

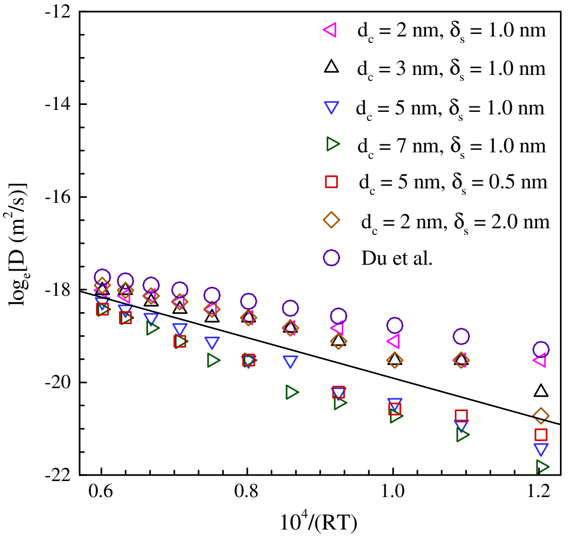

Fig. 14 Diffusion coefficient of nickel atoms in aluminum shell as a function of temperature for core diameters in the range of 2–7 nm and three different shell thicknesses of 0.5, 1.0, and 2.0 nm (*solid line* curve-fit $D = D_0 \exp(-E_A/RT)$, $E_A = 43.65$ kJ/mol, $D_0 = 1.77 \times 10^{-7}$ m^2/s)

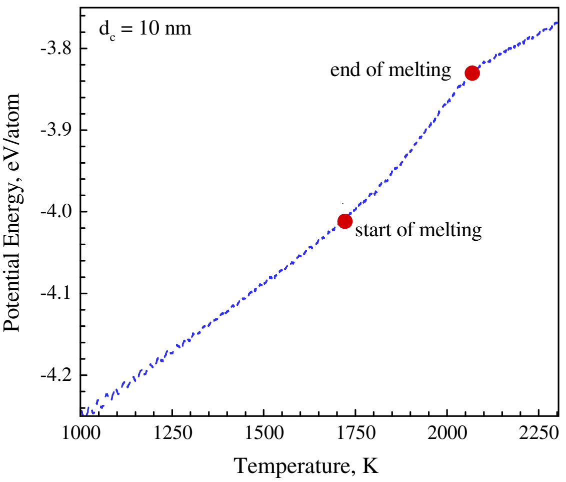

Fig. 15 Potential energy of the core as a function of temperature for a particle with core diameter of 10 nm and shell thickness of 1 nm

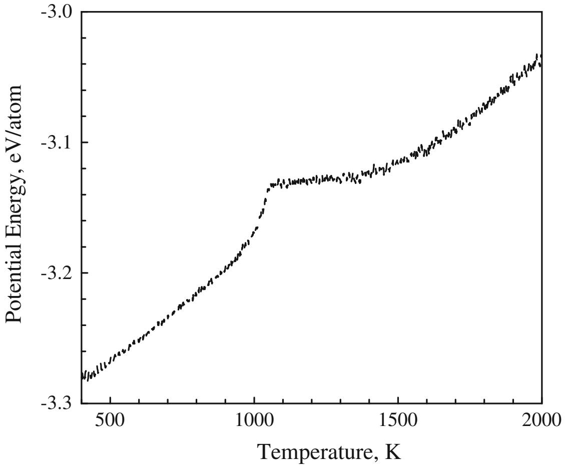

Fig. 16 Variation of potential energy with temperature for a particle with core diameter of 3 nm and shell thickness of 2 nm

Isochoric–isoenergetic MD simulations are performed to study inter-metallic reactions, which enables the particle to self-heat under adiabatic conditions. The calculated adiabatic reaction temperature is compared with the value obtained from thermodynamic energy balance analysis. Figure 17 shows the Ni–Al phase-equilibrium diagram (Massalski 1992). The product of nickel–aluminum reactions depends on the particle composition (Ni:Al atomic ratio) and temperature. In the present case, the inter-metallic reaction can be expressed as

$$10.72\mathrm{Al} + \mathrm{Ni} \rightarrow \mathrm{NiAl_3} + 7.72\mathrm{Al}. \tag{11}$$

The thermodynamic energy balance is given by

$$H_{\mathrm{reac}}(T_i) = H_{\mathrm{prod}}(T_{\mathrm{ad}}), \tag{12}$$

where H_{reac} is the enthalpy of the reactants at an initial temperature, T_i, and H_{prod} are the enthalpy of the products at the adiabatic reaction temperature, T_{ad}. The initial temperature is taken as 1,050 K.

The enthalpy of the reactants takes the form

$$H_{\mathrm{reac}} = 10.72 H_{\mathrm{Al}}^{1{,}050\,\mathrm{K}} + H_{\mathrm{Ni}}^{1{,}050\,\mathrm{K}} + 10.72 H_{\mathrm{m,Al}}. \tag{13}$$

The enthalpy of melting of aluminum is taken as 10.71 kJ/mol. The resulting reactant enthalpy is 327.8 kJ/mol. The total enthalpy of the products is expressed as

$$\begin{aligned} H_{\mathrm{prod}} = {} & \left(1 - \frac{t_i A}{V}\right) H_{\mathrm{f,NiAl_3}}^{298\,\mathrm{K}} \\ & + \left(C_{\mathrm{p,NiAl_3}} + 7.72 C_{\mathrm{p.Al}}\right)(T_{\mathrm{ad}} - 298) \\ & + H_{\mathrm{m,NiAl_3}} + 7.72 H_{\mathrm{m,Al}}, \end{aligned} \tag{14}$$

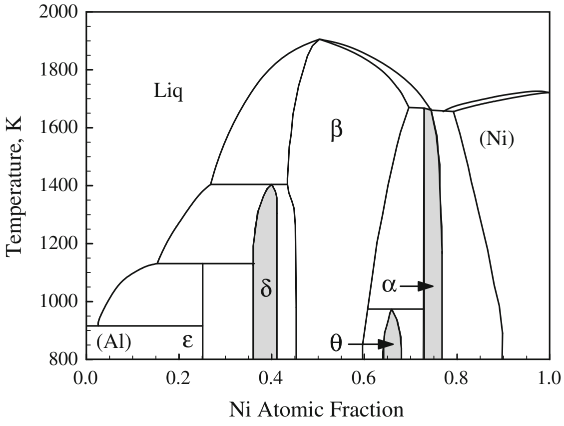

Fig. 17 Ni–Al phase diagram (ε: $\mathrm{NiAl_3}$, δ: $\mathrm{Ni_2Al_3}$, β: NiAl, θ: $\mathrm{Ni_5Al_3}$, and α: $\mathrm{Ni_3Al}$) (Massalski 1992)

where A is the interfacial area, V is the core volume, and t_i is the thickness of the interfacial zone. The interfacial core atoms participate in reactions prior to melting of the shell, thereby decreasing the particle energy content. The fraction of unreacted core volume depends on the interfacial area-to-volume ratio and thickness of the interfacial reaction zone. The latter is approximated to be 0.7 Å (Henz et al. 2009).The specific heat, enthalpy of melting, and heat of formation of $\mathrm{NiAl_3}$ are taken as 115 J/mol$^{-\mathrm{K}}$, 38 kJ/mol, and −150.6 kJ/mol, respectively (Morsi 2001). The reaction temperature calculated by equating (13) and (14) is 1,420 K. In other words, the particle is self-heated from 1,050 to 1,420 K due to the heat release from inter-metallic reactions. A more accurate result can be obtained by considering the size dependence of the heat of reaction, specific heat, and heat of fusion. Figure 18 shows the variation of the particle temperature with time under adiabatic conditions obtained using isochoric–isoenergetic MD simulations. The initial position and velocities of atoms are those obtained from the isobaric heating simulation at 1,050 K. The particle is heated from 1,050 to 1,540 K over a time period of 100 ps. Reasonably good agreement with the result of thermodynamic analysis is obtained. It is important to note that the atomic species are no longer expected to interact with a ground electronic configuration, but with an excited one at higher temperatures. Therefore, classical many-body potentials reproduce interaction forces with only modest accuracy, and ab initio methods should be applied.

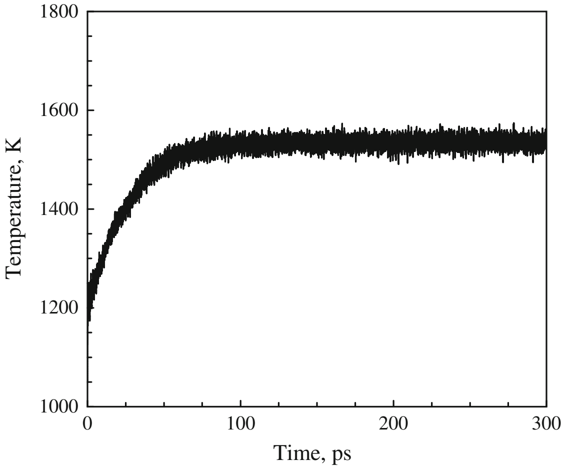

Fig. 18 Temporal variation of particle temperature under adiabatic condition for a core diameter of 3 nm and shell thickness of 2 nm; isochoric–isoenergetic MD simulations

It is useful to understand the effects of core diameter and shell thickness on the adiabatic reaction temperature of aluminum-coated nickel particles. Figure 19a shows the effect of shell thickness on the adiabatic reaction temperature for particles with a core diameter of 3 nm. The reaction temperature decreases from 1,850 to 1,350 K, when the shell thickness increases from 0.5 to 3.0 nm. This can be attributed to the changes in the composition of the reaction product. For a shell thickness of 0.5 nm, the alloying reaction takes the form

$$0.55\mathrm{Al} + 0.45\mathrm{Ni} \rightarrow \mathrm{Ni}_{0.45}\mathrm{Al}_{0.55}. \qquad (15)$$

As a result, all the atoms in the particles participate in the alloying reactions to form nickel–aluminum alloy. For thicker shells, the reaction can be expressed as

$$x\mathrm{Al} + \mathrm{Ni} \rightarrow \mathrm{NiAl}_3 + (x-3)\mathrm{Al}. \qquad (16)$$

The product thus contains unreacted aluminum atoms and aluminum-rich nickel–aluminum alloy. Satisfactory agreement with the results of thermodynamic analysis is obtained. Figure 19b shows the variation of the adiabatic reaction temperature with core diameter for particles with a shell thickness of 1 nm. It increases with increasing core diameter, attains a maximum value of ~2,050 K at 5 nm, and decreases with further increase in the core diameter. Chemical equilibrium analysis is performed to calculate the reaction temperatures of separated and core–shell particles. For separated particles, there is no energy loss due to interfacial pre-mixing process and the reaction temperatures are thus substantially greater than those obtained via MD simulations. Note that the reaction temperature is maximum when the particle composition favors the formation of the B2-NiAl, which has the highest heat of formation on a per mol-atom basis. Furthermore, the core size must be large enough to minimize the loss of energy content due to the interfacial pre-mixing process. Henz et al. conducted MD simulations and calculated the reaction temperatures of aluminum-coated nickel particles with equal number of aluminum and nickel atoms. The particle size range of concern was 3–9 nm. The reaction temperature increased with increasing core

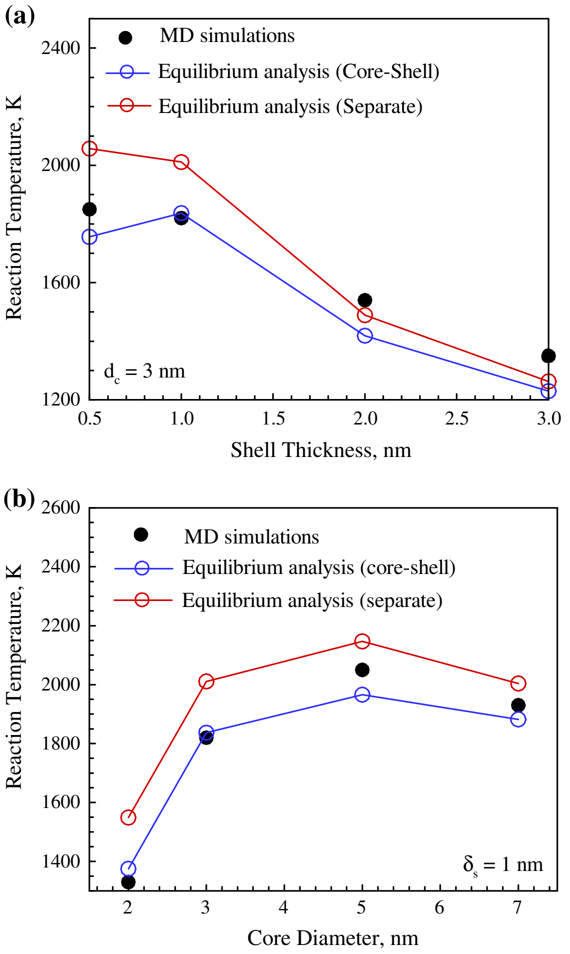

Fig. 19 Adiabatic reaction temperature of particles as a function of **a** shell thickness for a core diameter of 3 nm; **b** core diameter for a shell thickness of 1 nm

size, from 1,350 K at 3 nm to 1,525 K at 9 nm. This was attributed to the fact that the energy loss due to the interfacial pre-mixing process is greater for smaller particles. The reaction temperatures of Henz et al. are lower than those obtained in the present study. One possible reason is that a different potential function (Finnis–Sinclair potential) was employed to capture the interactions between atoms. Furthermore, the initial temperature was taken as 600 K, which is lower than those used in this study (800–1,000 K).

Particle burning time is another important property of concern. Figure 20 shows the effects of core diameter and shell thickness on the burning time of aluminum-coated nickel particles. The burning time exhibits core size dependence of the form

$$\tau_b = a d_c^n, \tag{17}$$

where d_c is the core diameter in nm, a is the pre-power factor, and n is the diameter exponent. For a shell thickness of 1 nm, n and a are calculated to be 1.70 and 4.97, respectively. The strong dependence of the burning time on particle size indicates the prevalence of diffusion-controlled conditions. The predicted diameter exponent is lower than the value of 2.5 obtained by Henz et al. The effect of shell thickness on the burning time is characterized by the following equation:

$$\tau_b = b\delta_s^m, \tag{18}$$

where δ_s is the shell thickness in nm, b is the pre-power factor, and m is the thickness exponent. For a core diameter of 3 nm, m and b are equal to 1.38 and 42.13, respectively. It is apparent that the core diameter and shell thickness dictate the physicochemical properties of aluminum-coated nickel particles. The calculated reaction time is in the range of 10–250 ps, while Henz et al. predicted significantly longer burning times (100–1,200 ps). Note that both the initial and final temperatures in Henz et al.'s study are lower than those in the present work. The diffusion coefficient decreases markedly with decreasing temperature, thereby resulting in longer burning times.

It is important to identify key results of the present study and discuss their general significance. For core–shell structured particles with a low melting point shell, the time period of concern can be divided into four stages. In the first stage, the particle is heated to the melting temperature of the shell. Diffusion of atoms and inter-metallic reactions are not significant in this stage. The solid-phase diffusion coefficients are in the order of 10^{-3} to 10^{-2} Å^2/ps, significantly lower than the liquid-phase counterparts (0.1–1 Å^2/ps). Melting of the shell, which marks the onset of the second stage, facilitates the diffusion of core and shell atoms. The diffusion process is accompanied by exothermic inter-metallic reactions which ignite the particle under adiabatic conditions. As a result, the particle ignition temperature is equal to the melting temperature of the shell, a size-dependent quantity. The melting temperature of the shell is weakly dependent on the core diameter, but decreases significantly with decreasing shell thickness. The diffusion

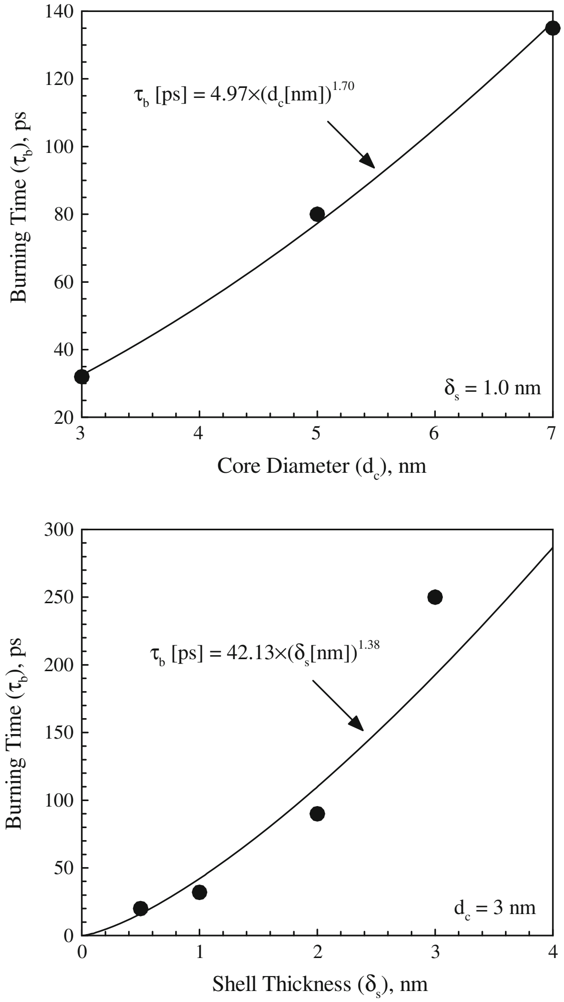

Fig. 20 Effects of core diameter and shell thickness on burning time of aluminum-coated nickel particles

process and inter-metallic reactions are thus promoted for particles with thinner shells. Deviation of the shell melting point from its bulk value is negligible for shell thickness >3 nm. Shell melting is a heterogeneous process in which the nucleation of the liquid phase begins at the outer surface of the particle. In the third stage, diffusion becomes more prominent and transforms the core–shell particle into a homogeneous alloy. The process is bidirectional, and the diffusion coefficients of core and shell atoms are nearly equal. For particles with a low melting point shell, the phenomenon of superheating of the core is not observed. The core melts at temperatures comparable to those of nascent particles. For smaller particles, alloying reactions compete with the melting process, and core melting is not clearly observable. The reaction temperature of a core–shell particle is a function of the core diameter and shell thickness. It becomes higher when the particle composition favors the formation of the product that has the highest heat of formation on a per mol-atom basis. Furthermore, the core must be large enough to minimize the loss of energy content due to the interfacial pre-mixing process. The particle burning time exhibits strong dependence of particle core size and shell thickness of the form $\tau_b = a\ d_c^n\ \delta_s^m$, with the exponents n and m being 1.70 and 1.38, respectively. The finding further corroborates the fact that the reaction rate of a core–shell particle is controlled by diffusion process.

Conclusions

Molecular dynamics simulations were performed to investigate the thermochemical behavior of aluminum-coated nickel particles in the size range of 4–13 nm, beyond which asymptotic behavior was observed. The atomic interactions were captured using an embedded atom model. Emphasis was placed on the particle melting behavior, diffusion characteristics, and inter-metallic reactions. Results were compared with the corresponding properties of nickel-coated nano-aluminum particles. Melting of the shell, which is a heterogeneous process beginning at the outer surface of the particle, was followed by diffusion of aluminum and nickel atoms and inter-metallic reactions. The ensuing chemical energy release significantly heated up the particle. The alloying reactions progressively transformed the core–shell structured particle into a homogeneous alloy. The melting temperature of the shell was weakly dependent on the core size, but increased significantly with increasing shell thickness, from 750 K at 1 nm to 1,000 K at 3 nm. The core melting behavior was in stark contrast to that observed for nickel-coated aluminum particles. The nickel core melted at a temperature comparable to the melting point of a nascent nickel particle, since the shell melted before the core. The melting point of the core decreased from 1,730 to 1,500 K, when its diameter decreased from 10 to 7 nm. For smaller cores, majority of nickel atoms diffused and reacted before melting occurs. The diffusion coefficient of nickel atoms in liquid aluminum shell exhibited a temperature dependence of the form $D = D_0 \exp(-E_A/RT)$, with an activation energy of 43.65 kJ/mol and pre-exponential factor of 1.77×10^{-7} m^2/s. The adiabatic reaction temperature increased with increasing core diameter, attained a maximum value of ~2,050 K at 5 nm, and decreased with further increase in the core diameter. The calculated values agreed reasonably well with those obtained via thermodynamic energy balance analysis. The burning time exhibited strong dependence of particle core size and shell thickness of the form $\tau_b = a\ d_c^n\ \delta_s^m$, with the exponents n and m being 1.70 and 1.38, respectively.

Acknowledgments The authors would like to thank the Air Force Office of Scientific Research (AFOSR) for their sponsorship of this program under Contract No. FA9550-11-1-0002. The support and encouragement provided by Dr. Mitat Birkan is greatly appreciated.

References

Andersen HC (1980) Molecular dynamics simulations at constant pressure and/or temperature. J Chem Phys 72:2384–2393

Andrzejak TA, Shafirovich E, Varma A (2007) Ignition mechanism of nickel-coated aluminum particles. Combust Flame 150:60–70

Aruna ST, Mukasyan AS (2008) Combustion synthesis and nanomaterials. Curr Opin Solid State Mater Sci 12:44–50

Baras F, Politano O (2011) Molecular dynamics simulations of nanometric metallic multilayers: reactivity of the Ni-Al system. Phys Rev B 84:024113

Du Y, Chang YA, Huang B, Gong W, Jin Z, Xu H, Yuan Z, Liu Y, He Y, Xie FY (2003) Diffusion coefficients of some solutes in FCC and liquid Al: critical evaluation and correlation. Mater Sci Eng 363:140–151

Eckert J, Holzer JC, Ahn CC, Fu Z, Johnson WL (1993) Melting behavior of nanocrystalline aluminum powders. Nanostruct Mater 2:407–413

Ejima T, Yamamura T, Uchida N, Matsuzaki Y, Nikaido M (1980) Impurity diffusion of fourth period solutes (Fe Co, Ni, Cu and Ga) and homovalent solutes (In and Tl) into molten aluminium. J Jpn Inst Met 44:316–323

Farber L, Klinger L, Gotman I (1998) Modeling of reactive synthesis in consolidated blends of fine Ni and Al powders. Mater Sci Eng A 254:155–165

Fischer SH, Grubelich MC (1996) A survey of combustion of metals, thermites, and intermetallics for pyrotechnic applications. AIAA Paper No. 96-3018

Fischer SH, Grubelich MC (1998) Theoretical energy release of thermites, intermetallics, and combustible metals. In: Proceedings of the international pyrotechnics seminar

Foley TJ, Johnson CE, Higa KT (2005) Inhibition of oxide formation on aluminum nanoparticles by transition metal coating. Chem Mater 17:4086–4091

Henz BJ, Hawa T, Zachariah M (2009) Molecular dynamics simulation of the energetic reaction between Ni and Al nanoparticles. J Appl Phys 105:124310

Huang Y, Risha GA, Yang V, Yetter RA (2009) Effect of particle size on combustion of aluminum particle dust in air. Combust Flame 156:5–13

Hunt EN, Plantier KB, Pantoya ML (2004) Nano-scale reactants in the self-propagating high-temperature synthesis of nickel aluminide. Acta Mater 52:3183–3191

Lai SL, Carlsoon JRA, Allen LH (1998) Melting point depression of Al clusters generated during the early stages of film growth: nanocalorimetry measurements. Appl Phys Lett 72:1098–1100

Levchenko EV, Evteev AV, Riley DP, Belova IV, Murch GE (2010) Molecular dynamics simulation of the alloying reaction in Al-coated Ni nanoparticle. Comput Mater Sci 47:712–720

Levitas VI, Samani K (2011) Size and mechanics effects in surface-induced melting of nanoparticles. Nat Commun 2:284

Li HP (2003) An investigation of the ignition manner effects on combustion synthesis. Mater Chem Phys 80:758–767

Lu SN, Ahrens TJ (2003) Superheating systematics of crystalline solids. Appl Phys Lett 82:1836–1838

Massalski TB (1992) Binary phase diagrams. ASM International, Materials Park

Mei QS, Lu K (2007) Melting and superheating of crystalline solids: from bulk to nanocrystals. Prog Mater Sci 52:1175–1262

Meschel SV, Kleppa OJ (2001) Thermochemistry of alloys of transition metals and lanthanide metals with some IIIB and IVB elements in the periodic table. J Alloys Compd 321:183–200

Morsi K (2001) Reaction synthesis processing of Ni–Al intermetallic materials. Mater Sci Eng A 299:1–15

Nose S (1984) A unified formulation of the constant temperature molecular dynamics methods. J Chem Phys 81:511–519

Papanicolaou NI, Chamati H, Evangelakis GA, Papaconstantopoulos DA (2003) Second-moment interatomic potential for Al, Ni and Ni–Al alloys, and molecular dynamics application. Comput Mater Sci 27:191–198

Politano O, Baras F, Mukasyan AS, Vadchenko SG, Rogachev AS (2013) Microstructure development during NiAl intermetallic synthesis in reactive Ni–Al nanolayers: numerical investigations vs TEM observations. Surf Coat Technol 215:485–492

Praizey JP, Garandet JP, Frohberg G, Griesche A, Kraatz KH (2000) Diffusion experiments in liquid metals. In: Proceedings of the first international symposium on microgravity research & applications in physical sciences and biotechnology, pp 481–490

Puri P, Yang V (2007) Effect of particle size on melting of aluminum at nano-scales. J Phys Chem C 111:11776–11783

Qi Y, Cagin T, Johnson WL, Goddard WA (2001) Melting and crystallization in Ni nanoclusters: the mesoscale regime. J Chem Phys 115:385–394

Reeves RV, Mukasyan AS, Son SF (2010) Thermal and impact reaction initiation in Ni/Al heterogeneous reactive systems. J Phys Chem C 114:14772–14780

Sundaram DS, Puri P, Yang V (2013) Thermochemical behavior of nickel-coated nanoaluminum particles. J Phys Chem C 117:7858–7869

Thiers L, Mukasyan AS, Varma A (2002) Thermal explosion in Ni–Al system: influence of reaction medium microstructure. Combust Flame 131:198–2009

Yih P (2000) U.S. Patent 6,010,610

Zhao S, Germann TC, Strachan A (2006) Atomistic simulations of shock-induced alloying reactions in Ni/Al nanolaminates. J Chem Phys 125:164707